Published online 28 July 2015

Nucleic Acids Research, 2015, Vol. 43, No. 16 ***8089–8099***
doi: 10.1093/nar/gkv760

Nucleotide binding interactions modulate dNTP selectivity and facilitate 8-oxo-dGTP incorporation by DNA polymerase lambda

Matthew J. Burak, Kip E. Guja and Miguel Garcia-Diaz*

Received March 17, 2015; Revised July 13, 2015; Accepted July 15, 2015

ABSTRACT

8-Oxo-7,8,-dihydro-2′-deoxyguanosine triphosphate (8-oxo-dGTP) is a major product of oxidative damage in the nucleotide pool. It is capable of mispairing with adenosine (dA), resulting in futile, mutagenic cycles of base excision repair. Therefore, it is critical that DNA polymerases discriminate against 8-oxo-dGTP at the insertion step. Because of its roles in oxidative DNA damage repair and non-homologous end joining, DNA polymerase lambda (Pol λ) may frequently encounter 8-oxo-dGTP. Here, we have studied the mechanisms of 8-oxo-dGMP incorporation and discrimination by Pol λ. We have solved high resolution crystal structures showing how Pol λ accommodates 8-oxo-dGTP in its active site. The structures indicate that when mispaired with dA, the oxidized nucleotide assumes the mutagenic *syn*-conformation, and is stabilized by multiple interactions. Steady-state kinetics reveal that two residues lining the dNTP binding pocket, Ala^{510} and Asn^{513}, play differential roles in dNTP selectivity. Specifically, Ala^{510} and Asn^{513} facilitate incorporation of 8-oxo-dGMP opposite dA and dC, respectively. These residues also modulate the balance between purine and pyrimidine incorporation. Our results shed light on the mechanisms controlling 8-oxo-dGMP incorporation in Pol λ and on the importance of interactions with the incoming dNTP to determine selectivity in family X DNA polymerases.

INTRODUCTION

DNA is vulnerable to damage by reactive oxygen species (ROS). Of the four nucleobases, guanine is the most susceptible to oxidative damage owing to its low redox potential (1). Moreover, guanine oxidation products have a high mutagenic potential (2–6). 8-oxo-7,8-dihydro-2′-deoxyguanosine (8-oxo-dG) is a major oxidative product present in cells and can arise in either DNA or the free nucleotide pool (7). Accordingly, oxidation of dGTP results in the formation of 8-oxo-7,8,-dihydro-2′-deoxyguanosine triphosphate (8-oxo-dGTP). Experimental measurements indicate that 8-oxo-dGTP may account for up to 10% of the total dGTP pool (8). In order to prevent the accumulation of 8-oxo-dGTP, cells encode a pyrophosphohydrolase, MutT/MTH1, which degrades the oxidized nucleotide (9–11). Despite expression of MutT/MTH1, nucleotide pools can accumulate enough 8-oxo-dGTP to promote mutagenesis and drive cancer progression (12,13). 8-oxo-dGTP is capable of adopting either an *anti* or *syn* conformation and thus can base-pair with either cytosine (dC) or adenine (dA), respectively (14–17). As a consequence of this, 8-oxo-dGTP is frequently misincorporated opposite dA *in vitro* by several DNA polymerases (18–25). Thus, *in vivo*, incorporation of 8-oxo-dGMP can lead to an A to C transversion mutation if left unrepaired (9). Conversely, 8-oxo-dGTP incorporation opposite dC can also eventually result in G to T tranversion mutations after subsequent replication (26).

All cells have specialized repair systems to deal with DNA modifications, and the base excision repair (BER) pathway is the main mechanism for purging the genome of oxidative lesions such as 8-oxo-dG (27). A specialized form of the BER pathway, initiated by the glycosylase MutY/MTYH, specifically recognizes and repairs 8-oxo-dG:dA mispairs by removing dA and replacing it with dC, enabling subsequent repair of the 8-oxo-dG lesion (28–31). However, no repair mechanism exists to cope with misincorporated 8-oxo-dGMP. Significantly, 8-oxo-dGMP misincorporation would lead to mutagenic repair by the MutY/MTYH-dependent BER pathway, directing removal of dA and not 8-oxo-dGMP. Thus, 8-oxo-dGMP misincorporation would unavoidably lead to mutagenesis, resulting an A to C transversion (26).

Therefore, preventing misincorporation of 8-oxo-dGMP outright is crucial to avoid mutagenesis. In addition to the hydrolytic activity of MutT/MUTH1, discrimination against 8-oxo-dGTP by DNA polymerases is an important factor in the prevention of mutagenesis. Therefore, understanding the mechanistic basis of this discrimination is of significant interest. With the exception of the recent characterization of the interaction between DNA polymerase beta (Pol β) and 8-oxo-dGTP (32,33), there is a lack of structural information that might help explain how DNA polymerases avoid 8-oxo-dGTP-induced mutagenesis.

*To whom correspondence should be addressed. Tel: +1 631 444 3054; Fax: +1 631 4449749; Email: miguel.garcia-diaz@stonybrook.edu

The family X DNA polymerase lambda (Pol λ) plays an important role in mediating cellular tolerance of guanine oxidation (34–36). A key element of the MutY/MTYH BER pathway is the ability to readily incorporate dCMP opposite a templating 8-oxodG. In the context of this repair reaction, Pol λ is uniquely capable of mediating faithful incorporation of dCMP to complete the repair (23). Pol λ also takes advantage of its unique catalytic properties to mediate additional roles in other DNA repair pathways related to oxidative damage, such as non-homologous end joining (NHEJ) (37–41).

Considering that Pol λ operates under conditions where oxidative damage is prevalent, it is expected to frequently encounter 8-oxo-dGTP. Moreover, due to its function in NHEJ, Pol λ may be responsible for mediating 8-oxo-dGTP-driven mutagenesis. Curiously, despite its relatively error-free behavior when faced with a templating 8-oxodG, Pol λ readily misinserts 8-oxo-dGMP opposite dA (23). The contrast between its behavior when incorporating 8-oxo-dGTP and opposite 8-oxo-dG indicates that the active site of Pol λ is asymmetrical, but the structural factors influencing 8-oxo-dGMP misincorporation by Pol λ are not well understood.

Here, we report high resolution pre- and post-catalytic crystal structures of Pol λ in complex with 8-oxo-dGTP and 8-oxo-dGMP, respectively. The structures demonstrate that the oxidized nucleotide can be accommodated in the Pol λ active site, where it is stabilized in the pro-mutagenic *syn*-conformation. Kinetic analysis demonstrates that two residues that partially conform the dNTP binding pocket influence 8-oxo-dGMP incorporation. Ala^{510} makes a Van der Waals interaction with the base of the incoming nucleotide, whereas Asn^{513} hydrogen-bonds with the C8-carbonyl. Our results indicate that Ala^{510} and Asn^{513} differentially impact 8-oxo-dGMP incorporation as well as the balance of purine/pyrimidine incorporation, confirming the importance of these residues in mediating nucleotide selectivity in family X DNA polymerases.

MATERIALS AND METHODS

Protein purification

The sequence corresponding to residues 242–575 of human Pol λ was previously cloned into the bacterial expression vector pET-22b (42). Site-directed mutagenesis was performed on the Pol λ expression vector to generate the A510D, N513A and A510D/N513A mutants. WT, A510D, N513A and A510D/N513A Pol λ were subsequently expressed in the *E. coli* strain BL21-CodonPlus(DE3)-RIL and purified as described (42).

Oligonucleotides for crystallography

Oligonucleotides used for the pre-catalytic ternary and post-catalytic nick complexes are shown in Supplementary Figure S1A and B respectively. Oligos were synthesized by solid-state synthesis methods using an automated DNA synthesizer. Oligos were subsequently purified by HPLC, ethanol precipitated and quantified by UV absorbance (A_{260}). P/T were annealed as previously described in 25 mM Tris–HCl pH 7.5 and 40 mM $MgCl_2$.

Crystallization

Pre-catalytic ternary complexes were formed using an upstream primer (UP5), downstream primer containing a 5′-phosphate group (DP4), and template (T8-A) (Supplementary Figure S1A). UP5, DP4 and T8-A (1:1:1) were heated to 80°C for 10 min before slowly cooling to room temperature in 25 mM Tris–HCl pH 7.5 and 50 mM $MgCl_2$. The resulting primer/templates (P/T) were mixed with WT Pol λ. However, due to the low melting temperature of DP-4 (16°C), a second annealing step in the presence of protein was used to ensure the proper formation of a 1-nt gapped substrate. Accordingly, the mixture was heated to 15°C for 5 min before slowly cooling to 4°C to ensure proper annealing of DP4. ddCTP and 8-oxo-dGTP/dTTP were sequentially added to the mixture in order to generate a pre-catalytic ternary complex. The resulting mixture (100 μl) contained 15 mM Tris–HCl pH 7.5, 75 mM NaCl, 10 mM $MgCl_2$, 1 mM DTT, P/T (0.5 mM), WT Pol λ (0.4 mM), 1 mM ddCTP and 3 mM 8-oxo-dGTP/dTTP. Crystals containing 8-oxo-dGTP were formed using the hanging drop method by mixing 2 μl of the protein/DNA solution containing DNA with 1 μl of the reservoir solution containing 0.1 M sodium cacodylate trihydrate pH 7.4 and 1.9 M sodium acetate trihydrate. The crystal was transferred to a solution containing 0.1 M sodium cacodylate trihydrate pH 7.4 and 1.9 M sodium acetate trihydrate and 25% (w/v) glycerol and cryo-cooled in liquid nitrogen prior to data collection. dTTP-containing crystals were formed as previously stated in solution containing 0.1 M sodium acetate trihydrate pH 4.6 and 2.0 M sodium formate. The crystal was transferred to a solution containing 0.1 M sodium acetate trihydrate pH 4.6 and 2.0 M sodium fomate and 25% w/v glycerol, harvested with a Mitegen MicroMount and cryo-cooled in liquid nitrogen prior to data collection.

Post-catalytic nick complexes were formed using an upstream primer (UP6), DP4 and template T8-A (Supplementary Figure S1B). Pre-hybridized UP6, DP4 and T8-A were mixed with WT Pol λ as previously described. 8-Oxo-dGTP (4 mM) was subsequently added and the resulting mixture (100 μl) was equilibrated for 60 min on ice in order to generate a post-catalytic nick complex. Crystals containing 8-oxo-dGMP were grown using the hanging drop method by mixing 1 μl of the protein/DNA solution containing DNA with 1 μl of the reservoir solution containing 0.1 M sodium citrate pH 5.6 and 1 M ammonium phosphate. The crystal was transferred to a solution containing 0.1 M sodium citrate pH 5.6, 1.2 M ammonium phosphate and 30% (w/v) glycerol, harvested with a Mitegen MicroMount and cryo-cooled in liquid nitrogen prior to data collection.

X-ray data collection and structure determination

Diffraction data were collected on beamline X25 of the National Synchrotron Light Source at Brookhaven National Laboratory for the dTTP pre-catalytic complex and the 8-oxo-dGTP post-catalytic complex, and on beamline 5.0.2 of the Advanced Light Source at Lawrence Berkeley National Laboratory for the 8-oxo-dGTP post-catalytic complex. All datasets were collected at 100 K using a wavelength of 1.0 Å. Diffraction data were processed using XDS (43) and Aimless (44) as implemented in the autoPROC pipeline

(45). Phases were obtained by molecular replacement using Phaser (46); search models for the pre- and post-catalytic complexes were created from 1XSN (47) and 1XSP (47), respectively. Model building was carried out in Coot (48), followed by refinement in Phenix (49), Refmac (50) and BUSTER (51). Diffraction data for the dTTP pre-catalytic complex were strongly anisotropic, with resolution limits (defined by $CC_{1/2}$ and $I/\sigma I$ (44,52) of 2.4 Å in a^* and c^* reciprocal space directions, but only 2.9 Å along the b^* direction. For this reason, an ellipsoidal truncation was carried out using the Anisotropy Diffraction Server (53). Briefly, data were truncated that fell outside an ellipse centered at the reciprocal lattice origin and having vertices at 1/2.4, 1/2.9, and 1/2.4 Å along a^*, b^*, and c^* axes, respectively. Isotropy was approximated by applying a negative scale factor along b^* (-16.8 Å^2) with no correction along a^* or c^*. These anisotropically scaled data then were used for refinement. In all three structures a small region of the protein surface, far removed from the active site (Loop 3) was disordered. The geometric quality of the refined models was assessed with MolProbity (54) and the structure validation tools in the Phenix suite. Data collection and refinement statistics are shown in Supplementary Table S1.

In order to facilitate more precise structural comparisons, a statistical analysis of atomic coordinate accuracy was carried out using SFCHECK (55). Following the method of Cruickshank (56), the standard deviation of the atomic coordinates can be derived from the properties of the electron-density map:

$$\sigma(x) = \sigma(\text{slope})/\text{curvature}$$

where σ(slope) and curvature are the standard deviation of the slope and curvature of the electron density map at the atomic center. The curvature is approximated by:

$$\text{curvature} = 2\pi^2\left(\sum h^2 F_{obs}\right)\Big/ a^2 V_{\text{unit\_cell}}$$

where a is the unit-cell length and h is the Miller index (57,58). The maximal expected coordinate error is calculated by expressing σ(slope) as a function of the difference between F_{obs} and F_{calc}

$$\sigma(\text{slope}) = 2\pi\left\{\sum\left[h^2\left(F_{\text{obs}} - F_{\text{calc}}\right)^2\right]\right\}^{1/2}\Big/ a V_{\text{unit\_cell}}$$

For any missing reflections, the program uses the average value of $\sigma(F)$ for the corresponding resolution shell instead of ($F_{\text{obs}} - F_{\text{calc}}$). The expected minimal coordinate error is estimated using the experimental $\sigma(F)$ instead of the difference between the observed and calculated structure factors. In this case σ(slope) is computed as

$$\sigma(\text{slope}) = 2\pi\left\{\sum\left[h^2\sigma(F)^2\right]\right\}^{1/2}\Big/ a V_{\text{unit\_cell}}$$

If there is no σ value for an observed structure factor, the program uses $\sigma = 0.04F_{\text{obs}}$ as the default value, which is roughly the error magnitude usually encountered. The both minimal and maximal estimated errors were calculated to account for the fact that the local quality of the electron density will amost always vary across different regions of a given crystal structure. These values are listed in Supplementary Table S2.

Oligonucleotides for steady-state primer extension assays

Oligonucleotides used for steady-state primer extension assays were obtained from Invitrogen and are shown in Supplementary Figure S1C and 1D. Oligos were purified by HPLC and polyacrylamide gel-electrophoresis (PAGE), quantified by UV absorbance (A_{260}), and heated to 80°C for 10 min before slowly cooling to room temperature overnight in 20 mM Tris–HCl pH 7.5 and 150 mM $MgCl_2$.

Steady-state primer extension assays

Steady-state experiments were performed with an upstream primer 5′ labeled with a Cy3 fluorophore (UP20), downstream primer containing a 5′-phosphate group (DP14), and a template (T35-A/T35-C) (Supplementary Figure S1C and 1D). The core sequence of P/T used was the same as the crystallography experiments. Pre-hybridized UP20, DP14 and T35-A/T35-C (1:1.2:1.2) were mixed with either WT A510D, N513A or A510D/N513A Pol λ. The resulting mixture (18 μl) contained 50 mM Tris–HCl pH 8.5, 10 mM $MgCl_2$, 1 mM DTT, 4% glycerol, 0.1 mg/ml BSA, P/T (200 nM) and either WT (0.3–5.0 nM), A510D (0.3–5.0 nM), N513A (0.3–5.0 nM) or A510D/N513A (0.5–10.0 nM) Pol λ. The protein/DNA mixture was directly added to varying amounts of either dTTP (0–500 μM), dGTP (0–500 μM) or 8-oxo-dGTP (0–1000 μM) to start the polymerization reaction.

Reaction mixtures (20 μl) were quenched by the addition of 95% (v/v) formamide, 10 mM EDTA, 0.001% xylene cyanol, 0.001% bromophenol blue (10 μl). Extended primers were separated by denaturing (8 M urea) 18% (v/v) PAGE. The fluorescence intensity of the bands was quantified using a Typhoon FLA 9000 imager and ImageQuant software.

Kinetic analysis of primer extension assays

The observed rate of nucleotide incorporation (extended primer) was plotted as a function of nucleotide concentration. Steady-state kinetic parameters, V_{max} and K_M, were determined by fitting the data to the Michaelis–Menten equation: $V = V_{\text{max}}[\text{S}]/(\text{K}_M + [\text{S}])$. k_{cat} was determined with the equation: $k_{\text{cat}} = V_{\text{max}}/[\text{E}]$.

RESULTS AND DISCUSSION

Pre-catalytic structure of Pol λ with an incoming 8-oxo-dGTP

In order to understand how 8-oxo-dGTP is misincorporated into DNA, we decided to solve a structure of Pol λ in complex with an incoming 8-oxo-dGTP in a pre-catalytic state. Thus, we crystallized Pol λ with a 1-nt gapped, dideoxy-terminated DNA substrate and an incoming 8-oxo-dGTP (Figure S1A). We obtained crystals that diffracted to a resolution of 1.95 Å. We were able to solve the structure using molecular replacement, and subsequent refinement converged to an R_{work} and R_{free} of 0.1999 and

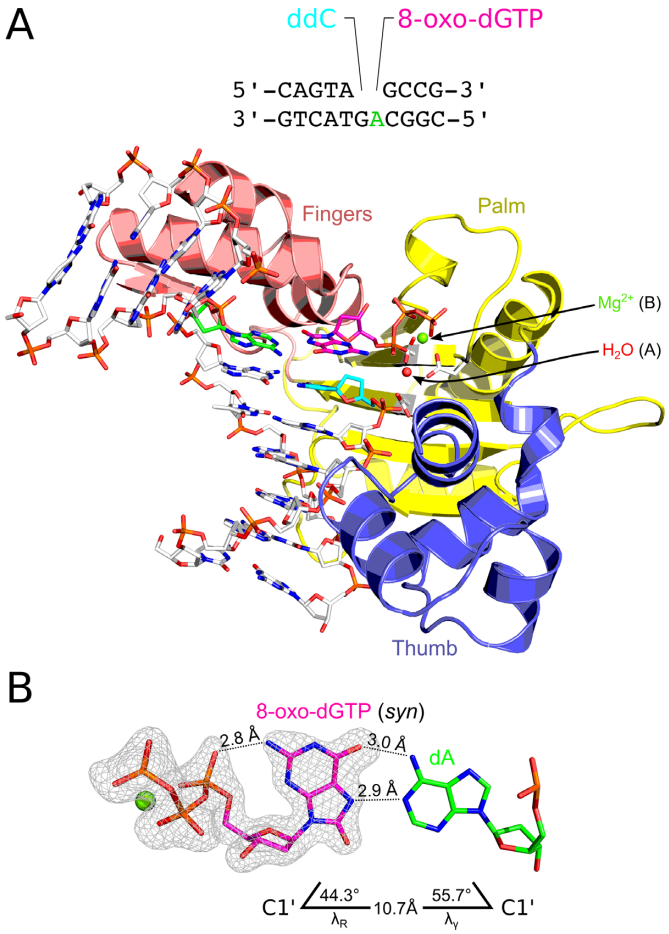

Figure 1. Pol λ pre-catalytic complex for 8-oxo-dGTP. (**A**) The 39-kDa catalytic domain (8-kDa subdomain not shown for clarity) is colored by subdomain: fingers (salmon), palm (yellow) and thumb (purple). The polymerase is in complex with 8-oxo-dGTP (magenta) and a 1-nt gapped 16-mer P/T (gray). The upstream primer is terminated with a dideoxynucleotide (ddC) (cyan). (**B**) 8-Oxo-dGTP (magenta) establishes a Hoogsteen basepair with dA (green). Contoured at 3σ, the simulated annealing $F_o - F_c$ omit density map (gray) for 8-oxo-dGTP is shown. The geometry (C1′ distance and λ angles) of the mismatched base-pair is indicated at the bottom of the figure.

0.2273 respectively (Supplementary Table S1). The electron density was of sufficient quality to build protein residues 252–575 and all DNA bases, including the incoming 8-oxo-dGTP. Inspection of the structure immediately reveals that, as expected, 8-oxo-dGTP is bound in the active site (Figure 1A). A Mg^{2+} atom is present in the dNTP-binding metal (B) site. However, a water molecule is occupying the site of the catalytic metal (A), consistent with the absence of the 3′OH group from the nucleotide at the primer terminus (47) (Figure 1A).

The density for the 8-oxo-dGTP residue is of high quality, and the C8 carbonyl is clearly observed (Figure 1B). The structure indicates that the incoming 8-oxo-dGTP adopts a *syn*-conformation and forms a Hoogsteen base-pair with the templating adenine base. Hydrogen-bonds are established between N6 of the adenine and O6 of the guanine (3.0 Å) and N1 of the adenine and N7 of the guanine (2.9 Å). An intramolecular hydrogen-bond between the N2 and a non-bridging oxygen on the α-phosphate of 8-oxo-dGTP may stabilize the *syn*-conformation. These interactions and the geometry of 8-oxo-dGTP in the active site of Pol λ are consistent with the conformation observed in existing structures of Pol β in complex with 8-oxo-dGTP (32,33).

Interestingly, the geometry of the 8-oxo-dGTP:dA mispair differs from a canonical Watson-Crick base-pair. The λ_R angle for 8-oxo-dGTP is 44.3° which is consistent with the *syn*-conformation of the base in other reported structures (Pol β – 44.2°) (32,33). However, this differs from that of a dGMPCPP:dC base-pair (54.2°) (59). The λ_γ angle for dA is 55.7° and is consistent with an ddTTP:dA base-pair (1XSN) (47). This is in agreement with the idea that 8-oxo-dG adopts an alternate conformation in order to mispair with an adenosine (15,16). Also, the C1′–C1′ width of the mispair is 10.7 ± 0.015–0.091 Å (where 0.015 and 0.091 Å correspond to the minimum and maximum estimated errors respectively, Supplementary Table S2) which is larger than for a dTTP:dA base-pair (10.5 ± 0.021–0.094 Å, Supplementary Table S2). Interestingly, this larger base pair width appears to be correlated with the presence of a mispair in the active site in Pol λ (dGMPCPP:dT, 10.8 Å) (59). However, despite these distortions, Pol λ can accommodate the 8-oxo-dGTP:dA mispair in the active site without any major conformational rearrangements, as evidenced by the small RMSD between our structure and a reference pre-catalytic complex containing a ddTTP:dA base-pair in the active site (1XSN, RMSD of 0.320 Å over 261 Cα atoms) (47).

Post-catalytic structure of Pol λ with incorporated 8-oxo-dGMP

The absence of large-scale subdomain conformational motions during catalysis in Pol λ implies that completion of the nucleotidyl transfer reaction and advancement from pre-catalytic to the post-catalytic complex involves no significant conformational changes, other than stereochemical inversion of the α-phosphate (47). We therefore took advantage of this fact in order to determine whether our structure indeed represents a catalytically relevant conformation of 8-oxo-dGTP. We decided to crystallize a post-catalytic complex of Pol λ with a nicked DNA substrate containing an 8-oxo-dG moiety at the primer terminus (Figure 2A). The crystals of the post-catalytic complex diffracted to a resolution of 2.15 Å. The structure was solved by molecular replacement, and refinement converged to an R_{work} and R_{free} of 0.2144 and 0.2450, respectively (Supplementary Table S1). The electron density was of sufficient quality to build protein residues 251–575 and all DNA bases, including the incorporated 8-oxo-dGMP.

The post-catalytic structure contains both products of the phosphoryl transfer reaction (47). In the structure, 8-oxo-dGTP has been turned over, and the incorporated 8-oxo-dGMP maintains the *syn*-conformation. However, the pyrophosphate released by the reaction has diffused away from the active site and has been replaced by a citrate ion. Citrate is present in high concentration in the crystallization buffer and mimics the conformation of pyrophosphate in other post-catalytic structures (47). Additionally, the citrate is coordinating a Na^+ ion that is present in the metal B site (Figure 2A). The metal A is absent in the structure,

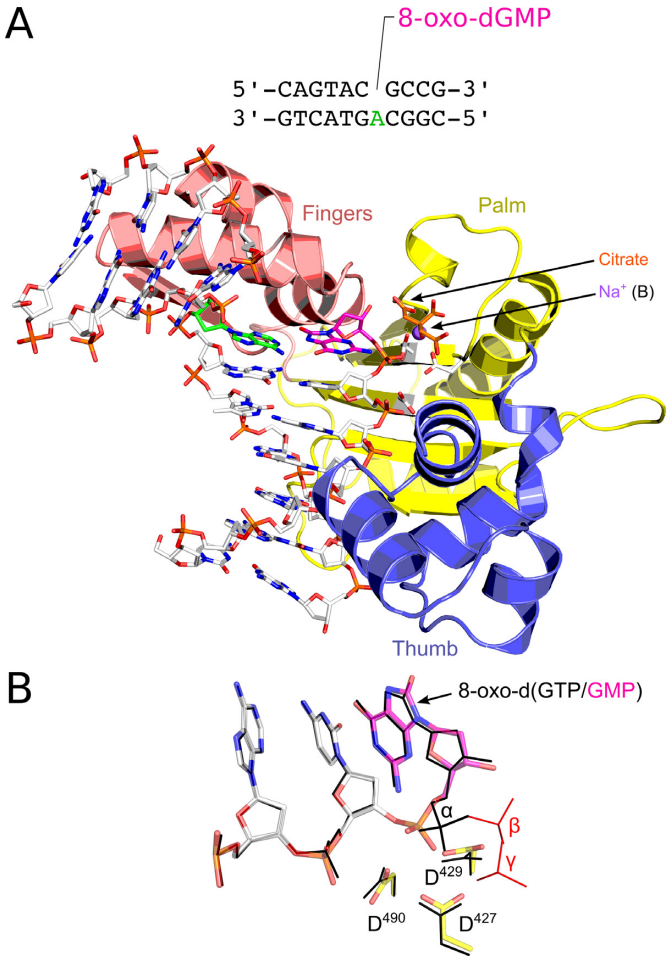

Figure 2. Pol λ post-catalytic complex for 8-oxo-dGMP incorporation. (**A**) The 39-kDa catalytic domain (8-kDa subdomain not shown for clarity) is colored by subdomain: fingers (salmon), palm (yellow) and thumb (purple). The polymerase is in complex with a nicked 16-mer P/T (gray) containing an 8-oxo-dGMP moiety at the primer terminus (magenta). (**B**) Overlay of the active sites between the pre- and post-catalytic 8-oxo-dGTP/8-oxo-dGMP complexes (RMSD of 0.278 Å over 678 Cα atoms). The β- and ϒ-phosphates that will constitute the pyrophosphate leaving group are highlighted in red.

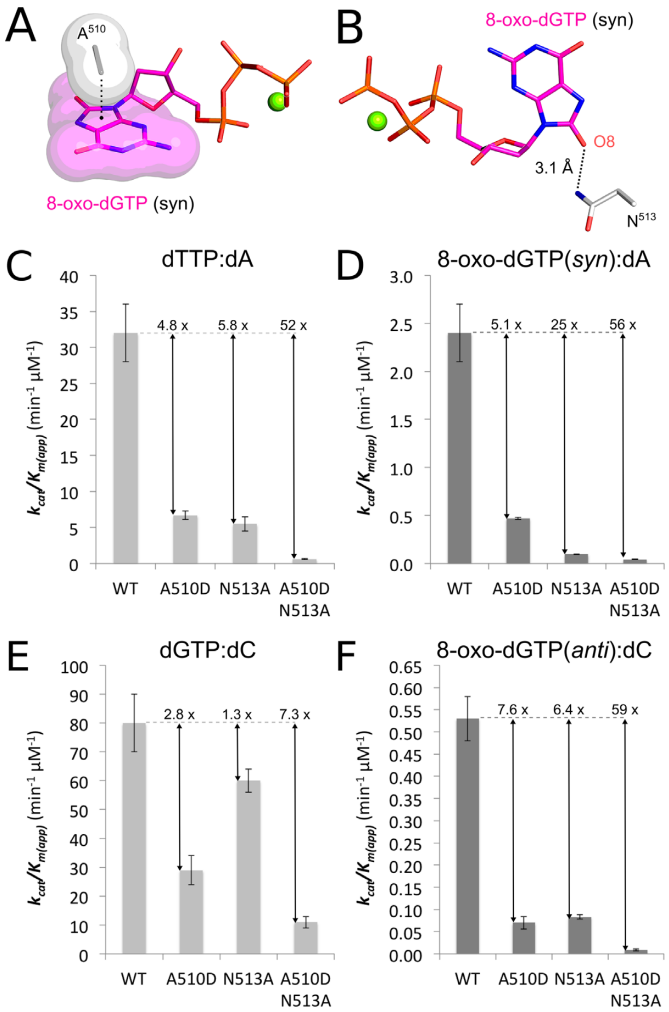

Figure 3. Structural features that promote 8-oxo-dGTP incorporation. (**A**) Ala^{510} provides a Van der Waals stacking interaction with the nucleotide of the incoming 8-oxo-dGTP (magenta). (**B**) Asn^{513} stabilizes 8-oxo-dGTP (magenta) in the *syn*-conformation. The amino group of the Asn^{513} side chain establishes a hydrogen-bond with the O8 of 8-oxo-dGTP. (**C**) Comparison of catalytic efficiencies for dTMP incorporation opposite dA using WT, A510D, N513A and A510D/N513A Pol λ. (**D**) Comparison of catalytic efficiencies for 8-oxo-dGMP(*syn*) incorporation opposite dA using WT, A510D, N513A and A510D/N513A Pol λ. (**E**) Comparison of catalytic efficiencies for dGMP incorporation opposite dC using WT, A510D, N513A and A510D/N513A Pol λ. (**F**) Comparison of catalytic efficiencies for 8-oxo-dGMP(*anti*) incorporation opposite dC using WT, A510D, N513A and A510D/N513A Pol λ.

consistent with the notion that it dissociates after nucleotide incorporation (47). Superimposition of the pre- and post-catalytic structures reveals that both complexes adopt similar conformations (RMSD of 0.238 Å over 236 Cα atoms). Furthermore, the geometry of all active site atoms is conserved (Figure 2B). This confirms that the conformations seen in our structures are catalytically relevant.

8-Oxo-dGTP is stabilized by numerous interactions

Close inspection of the dNTP binding pocket reveals five residues that interact with 8-oxo-dGTP (Supplementary Figure S2). Three residues form hydrogen-bonding interactions with non-bridging phosphate oxygen atoms in the incoming nucleotide. Arg^{386} forms a bidentate hydrogen-bond (3.0 and 3.2 Å) with the γ-phosphate while Ser^{417} and Arg^{420} each form a hydrogen-bond with the γ-phosphate (2.6 Å) and the β-phosphate (3.0 Å), respectively. Together, these three residues form the phosphate-binding pocket for the incoming nucleotide. However, these interactions are unlikely to confer specificity, since they are established irrespective of the identity of the incoming nucleotide.

Ala^{510} provides a Van der Waals stacking interaction with the oxidized nucleobase (Figure 3A). This interaction is analogous to what is observed in a complex with undamaged substrates, and is thought to be responsible for the high dNTP binding affinity of Pol λ (60). It is however conceivable that the strength of the Ala^{510} interaction depends on the identity of the incoming dNTP. Consistent with this idea, Ala^{510} was shown to help discriminate against incorrect nucleotide binding (61). Thus, Pol λ may rely on Ala^{510}

to probe for proper nascent base-pair geometry of 8-oxo-dGTP.

In addition to Ala^{510}, another residue recognizes a unique structural characteristic of 8-oxo-dGTP. Asn^{513} forms a hydrogen-bonding interaction (3.1 Å) with the C8-carbonyl of 8-oxo-dGTP (Figure 3B). In the Pol λ active site, Asn^{513} establishes a sequence independent hydrogen-bond with the O2/N3 hydrogen-bond acceptors in the minor groove of the incoming nucleotide (42). These types of minor groove interactions are thought to be crucial to the ability of DNA polymerases to discriminate against non-Watson–Crick base pairs and thus promote fidelity of synthesis (62,63). Similar to what is observed with 8-oxo-dG in the active site of different polymerases (64–67), 8-oxo-dGTP may hijack this fidelity checkpoint mechanism in order to stabilize *syn*-dependent misincorporation. The O8 of 8-oxo-dGTP (*syn*) in the DNA minor groove is in a position similar to that of O2 of dTTP for a canonical Watson-Crick base-pair. This suggests that Asn^{513} stabilizes the lesion in the *syn*-conformation and thus mediates misincorporation opposite dA. Asn^{513} is conserved in another family X DNA polymerase, human Pol β, where it plays a critical role in facilitating incorporation of 8-oxo-dGMP opposite template dA (19,32,33). Our structural data suggest that this residue could play a similar role in Pol λ.

Steady-state kinetic analysis of the relevance of Ala^{510} for 8-oxo-dGTP incorporation

As mentioned above, our structural results reveal that 8-oxo-dGTP is stabilized by two specific interactions. One of these, Ala^{510}, provides a Van der Waals stacking interaction with the nucleobase of 8-oxo-dGTP. Interestingly, Ala^{510} in Pol λ is replaced by an aspartic acid in Pol β (Asp^{276}), which is believed to restrict dNTP binding (68,69). Thus, to further characterize the role of Ala^{510} on 8-oxo-dGTP misincorporation in Pol λ, we constructed an A510D active-site substitution and performed a steady-state kinetic analysis.

Previous data had determined the catalytic efficiency of incorporation of 8-oxo-dGMP opposite dA and dC (23). However, these studies lacked a comparison to dTMP incorporation. This is relevant, since 8-oxo-dGMP competes with dTTP for binding opposite a templating dA, and thus the relative incorporation efficiency of the two nucleotides ultimately determines the mutagenic potential of 8-oxo-dGTP *in vivo*. In order to avoid possible sequence-related effects, the core sequence of the P/T used was identical to that of the oligos used for crystallography (Supplementary Figure S1C and 1D). Using these substrates we determined the kinetic parameters [k_{cat} and $K_{m(app)}$] and catalytic efficiencies [$k_{cat}/K_{m(app)}$] for both WT and A510D Pol λ (Table 1).

A comparison of the catalytic efficiencies for WT Pol λ revealed a 150-fold difference between dGMP and 8-oxodGMP incorporation opposite dC. Conversely, incorporation of 8-oxo-dGMP was only 13-fold less efficient than dTMP opposite dA. The relatively small difference in catalytic efficiencies for 8-oxo-dGMP and dTMP incorporation opposite dA highlights the mutagenic potential of this lesion. Furthermore, comparison of the dA/dC selectivity for 8-oxo-dGTP also revealed that the pro-mutagenic *syn*-conformation is preferred in WT Pol λ (5:1).

Interestingly, the A510D substitution had a differential effect on all nucleotides tested. With respect to WT protein, dTTP and 8-oxodGTP incorporation opposite dA was reduced by 4.8-fold (Figure 3C) and 5.1-fold (Figure 3D), respectively. This suggests that the A510D substitution may affect 8-oxo-dGTP(*syn*) in a similar manner to dTTP. However, the same does not hold true for dGTP/8-oxo-dGTP opposite dC. Notably, the A510D substitution had the largest effect on the incorporation of 8-oxo-dGTP opposite dC (7.6-fold, Figure 3E) as opposed to dGTP (2.8-fold, Figure 3F). This suggests that Ala^{510} may preferentially stabilize the *anti*-conformation of 8-oxo-dGTP, promoting its incorporation opposite dC. Accordingly, Ala^{510} may enhance the ability of Pol λ to incorporation 8-oxo-dGMP opposite dC, which could ultimately increase the frequency of G to T tranversion mutations (26).

Steady state kinetic analysis of the relevance of Asn^{513} on 8-oxo-dGTP incorporation

In addition to Ala^{510}, Asn^{513} also makes a specific interaction with the oxidized nucleobase. To characterize the role of Asn^{513} on 8-oxo-dGTP misincorporation in Pol λ, we generated a N513A active-site substitution. Steady-state kinetic parameters [k_{cat} and $K_{m(app)}$] and catalytic efficiencies [$k_{cat}/K_{m(app)}$] for dTTP/8-oxo-dGTP incorporation opposite dA and dGTP/8-oxo-dGTP opposite dC were determined using N513A Pol λ (Table 1). Given the importance of Asn^{513} during normal polymerization, the N513A substitution expectedly affected the catalytic efficiency for all nucleotides tested. Interestingly, similar to what was observed with Ala^{510}, the effects were differential for all nucleotides tested. With respect to the WT protein, the catalytic efficiency for dTTP decreased by 5.8-fold (Figure 3C) in N513A Pol λ. However, the N513A substitution resulted in a much more drastic effect in the context of 8-oxo-dGMP incorporation opposite dA (25-fold, Figure 3D). Also, the catalytic efficiencies of dGMP and 8-oxo-dGMP incorporation opposite dC were reduced by 1.3 (Figure 3E) and 6.4-fold (Figure 3F) respectively. Taken together, these results suggest that Asn^{513} plays an important role in facilitating 8-oxo-dGMP incorporation opposite dA, implying that this residue selectively stabilizes the *syn*-conformation of 8-oxo-dGTP.

Our results suggest that dNTP binding by Pol λ is influenced by multiple amino acid residues. Moreover, both Ala^{510} and Asn^{513} appear to play critical roles for *anti*/*syn*-discrimination. To examine if these residues behave individually or cooperatively, we created a A510D/N513A double substitution (Table 1, Figure 3C–F). As expected, the effects of both substitutions synergistically impacted all nucleotides tested. Interestingly, the drop in catalytic efficiency was nearly identical for 8-oxo-dGMP incorporation opposite dA and dC. This is consistent with the opposite effects of Ala^{510} and Asn^{513}, facilitating incorporation of the *anti*- and *syn*-conformations, respectively.

Table 1. Steady-state kinetic parameters of incorporation of 8-oxo-dGTP opposite dA and dC by DNA polymerase lambda

Protein	Template	dNTP	K_M (μM)	k_{cat} (min^{-1})	k_{cat}/K_M (min^{-1} μM^{-1})
WT	A	dTTP	4.2 ± 0.7	131 ± 7	32 ± 4
		8-oxo-dGTP	20 ± 3	45.2 ± 3.9	2.4 ± 0.3
A510D		dTTP	35 ± 4	234 ± 10	6.7 ± 0.6
		8-oxo-dGTP	120 ± 8	56.8 ± 2.8	0.47 ± 0.01
N513A		dTTP	21 ± 4	113 ± 1	5.5 ± 1.0
		8-oxo-dGTP	41 ± 1.6	3.99 ± 0.06	0.097 ± 0.003
A510D N513A		dTTP	120 ± 16	71.8 ± 5.6	0.62 ± 0.07
		8-oxo-dGTP	71 ± 2	3.00 ± 0.41	0.043 ± 0.005
WT	C	dGTP	1.7 ± 0.1	140 ± 22	80 ± 10
		8-oxo-dGTP	8.4 ± 0.8	4.39 ± 0.04	0.53 ± 0.05
A510D		dGTP	2.8 ± 0.5	80.0 ± 6.8	29 ± 5
		8-oxo-dGTP	24 ± 6	1.53 ± 0.05	0.070 ± 0.014
N513A		dGTP	2.0 ± 0.2	121 ± 2	60 ± 4
		8-oxo-dGTP	16 ± 0.47	1.31 ± 0.05	0.083 ± 0.005
A510D N513A		dGTP	6.3 ± 0.8	67.2 ± 1.3	11 ± 2
		8-oxo-dGTP	120 ± 24	1.06 ± 0.04	0.009 ± 0.002

*Each experiment was independently repeated. Reported results are mean ± SD from three independent experiments.

Structural features in Pol λ discourage 8-oxo-dGTP misincorporation

Although the 8-oxo-dGTP:dA mispair is tolerated in the active site of Pol λ, kinetic analysis indicates that the insertion efficiency is reduced relative to that of a Watson–Crick base-pair (Table 1). In order to determine the structural features discouraging incorporation of 8-oxo-dGTP we crystallized Pol λ in complex with undamaged DNA in the exact same sequence context (Supplementary Table S1). We rationalized that this would provide a more accurate basis for comparison to the 8-oxo-dGTP containing structure, since existing structural models either lacked a 3′-OH on the incoming nucleotide (1XSN) (47), or used a non-hydrolyzable dNTP analog to trap the ternary complex (2PFO) (70). The crystals diffracted with strong anisotropy, to a resolution limit of 2.4 Å in *a** and *c** reciprocal space directions, but only 2.9 Å along the *b** direction. For this reason, an anisotropic correction was carried out using the Anisotropy Diffraction Server [PMID: 24203335]. The structure was solved with molecular replacement and the model was refined to convergence (R_{work}/R_{free}: 0.1874/0.2358). The electron density was of sufficient quality to build protein residues 252–575 and all DNA bases, including the incoming dTTP.

Comparing our precatalytic structure for 8-oxo-dGMP incorporation with this structure indicates that the overall fold of the polymerase is conserved (RMSD of 0.418 over 289 Cα atoms). However, closer inspection of the active site reveals some important differences. First, the 8-oxo-dGTP does not appear to stack as well as dTTP with the base at the primer terminus (Figure 4A). In an attempt to maximize this stacking interaction and accommodate 8-oxo-dGTP in the active site, the templating adenine shifts 0.3 Å away from the incoming nucleotide (Figure 4B). The direct consequence of this distortion places the templating base 0.4 Å away from the minor groove interacting residue, Arg^{517} (Figure 4B).

Arg^{517} plays an important role interrogating the nascent base-pair conformation. This residue forms a hydrogen-bond with the templating base and adopts a base-pair checking conformation in response to dNTP binding (47).

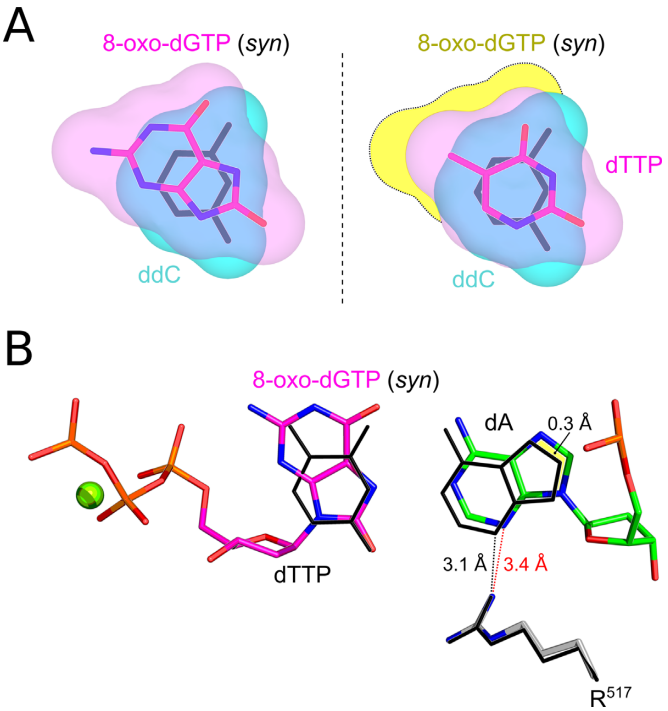

Figure 4. Structural features that discourage incorporation. (**A**) Comparison of dTTP and 8-oxo-dGTP stacking interactions in the pre-catalytic structures. The stacking interaction between 8-oxo-dGTP(*syn*) (magenta) and ddC (cyan) at the primer terminus of a complex is shown in the left panel. Comparison with dTTP (magenta) and the ddC (cyan) in the right panel demonstrates that 8-ox-dGTP stacks more poorly (yellow). (**B**) Overlay of the nascent base-pair in the pre-catalytic 8-oxo-dGTP and dTTP complexes. 8-oxo-dGTP (magenta) appears to displace the templating dA away from its canonical position. The direct consequence of this is that dA shifts further away from Arg^{517}. The hydrogen-bonding distances for the pre-catalytic 8-oxo-dGTP and dTTP complexes are shown in black and red respectively.

This mechanism appears to be critical for fidelity of synthesis in family X polymerases. Consistently, substitution of Arg^{517} in Pol λ sharply decreases the fidelity of the polymerase as well as the catalytic efficiency of dNTP incorpo-

ration (61). Similarly, even subtle alterations of this residue in Pol β result in substantial reduction in the catalytic efficiency (71). Thus, repositioning of the templating adenosine away from Arg^{517} as observed in our structure would likely cause a loss of insertion efficiency. This provides a structural explanation for the decreased incorporation efficiency observed in our kinetic analysis (Table 1).

Ala^{510} and Asn^{513} influence the purine/pyrimidine balance in Pol λ

While Asn^{513} enhances 8-oxo-dGTP incorporation in Pol λ, this residue also had a differential effect on dTTP and dGTP incorporaton. Steady-state kinetic analysis demonstrated that the catalytic efficiency for dTTP incorporation by N513A Pol λ was 5.8-fold (Figure 3C) lower than WT, whereas the decrease observed in the case of dGTP incorporation was just 1.3-fold (Figure 3E). Interestingly, the equivalent residue in the family X DNA polymerase from the heat-stable organism *T. thermophilus* (TthPolX) appears to also influence the balance of purine/pyrimidine incorporation (72). Asn^{513} appears to play a similar role in balancing the purine/pyrimidine bias in Pol λ.

Strikingly, Ala^{510} also appears to have a greater effect on pyrimidines than purines. A510D substitution results in a 4.8-fold (Figure 3C) decrease in catalytic efficiency for dTTP incorporation but only a 2.8-fold (Figure 3E) decrease for dGTP. In agreement with these results, the A510D/N513A double mutant displays a clear synergistic effect. The double substitution affects dTTP incorporation to a far greater extent (52-fold, Figure 3C) than dGTP (7.3-fold, Figure 3E), demonstrating that both residues contribute to balancing purine/pyrimidine incorporation in Pol λ. This indicates that residues in addition to Asn^{513} are important to achieve the correct purine/pyrimidine balance.

CONCLUSION

The free nucleotide pool is susceptible to oxidative damage (73). To cope with this oxidative burden, cells encode an enzyme (MutT/MTH1) to sanitize the nucleotide pools by degrading oxidized nucleotides such as 8-oxo-dGTP (10,11). Despite the presence of this protein, residual 8-oxo-dGTP is still capable of promoting mutagenesis (8,12,13). As a result, DNA polymerases such as Pol λ may encounter and incorporate this oxidized nucleotide, ultimately leading to mutagenesis.

The structural and kinetic studies presented here reveal how 8-oxo-dGTP evades fidelity checkpoint mechanisms in Pol λ. Active site residues Ala^{510} and Asn^{513} establish critical interactions that help stabilize the incoming nucleotide during polymerization. Asn^{513} forms a minor groove interaction with the incoming nucleotide. While this interaction is used to ensure that a base-pair with the proper geometry is formed in the active site of the polymerase (42,47), this mechanism is co-opted by 8-oxo-dGTP and appears to drive its mutagenic incorporation opposite dA. Asn^{513} is capable of forming a hydrogen-bond with the C8-carbonyl of 8-oxo-dGTP, thereby stabilizing the oxidized nucleotide in a *syn*-conformation. Consistently, substitution of asparagine to an alanine eliminates the stabilizing hydrogen-bond and results in a 25-fold reduction in the catalytic efficiency for 8-oxo-dGTP misincorporation opposite dA. Conversely, the N513A substitution has only a minor effect on dTTP incorporation opposite dA (5.8-fold). Thus, Asn^{513} appears to selectively facilitate 8-oxo-dGMP misincorporation.

Asn^{513} is also conserved in another family X DNA polymerase, Pol β (Asn^{279}). Accordingly, Asn^{279} also appears to play a role mediating 8-oxo-dGTP-induced mutagenesis. Strikingly, in comparison to Pol β (1000-fold), the effects of Asn^{513} on 8-oxo-dGMP misincorporation in Pol λ are far less pronounced (25-fold) (19). This implies that minor groove interactions are less critical to stabilize 8-oxo-dGTP in a *syn*-conformation in the Pol λ active site. The lesser relative importance of Asn^{513} with respect to Asn^{279} is perhaps owed to the differential interactions established by Pol λ with the incoming nucleotide. Pol λ has a higher binding affinity for nucleotides than Pol β (60), which is thought to be largely the result of a Van der Waals contact established between Ala^{510} and the incoming nucleobase. Conversely, the equivalent residue in Pol β, Asp^{276}, is believed to restrict dNTP binding (68,69).

Our results demonstrate that Ala^{510} substitution differentially affects incorporation of the nucleotides tested. This implies that Ala^{510} establishes distinct interactions with each nucleotide and therefore is unequally responsible for their stability in the active site. While an A510D substitution had an nearly equivalent effect on both dTTP (4.8-fold) and 8-oxo-dGTP(*syn*) (5.1-fold), one consequence of this behavior is that substitution of Ala^{510} selectively impacts 8-oxo-dGTP misincorporation opposite dC. Substitution of Ala^{510} to aspartic acid results in a greater effect on 8-oxo-dGMP incorporation (7.6-fold) opposite dC than dGMP (2.8-fold). This may be due to an unfavorable electrostatic interaction between the side chain and the C8-carbonyl of the nucleotide. As a consequence, Ala^{510} selectively enhances the incorporation of 8-oxo-dGMP opposite dC. These results are consistent with the increased propensity of 8-oxo-dGTP incorporation opposite dA relative to dC by Pol λ (5:1) in comparison to Pol β (24:1) (19,23). Furthermore, this implies that Pol λ may be more susceptible to G to T transversion mutations induced by 8-oxo-dGMP incorporation opposite dC than Pol β.

Curiously, the effects of Ala^{510} and Asn^{513} on normal nucleotide incorporation appear to have a more pronounced effect on dTMP than dGMP incorporation. The A510D substitution results in a greater effect for dTTP (4.8-fold) incorporation than dGTP (2.8-fold). Likewise, a N513A substitution has a more prominent effect on dTTP (5.8-fold) incorporation than dGTP (1.3-fold). Interestingly, the family X DNA polymerase from the heat-stable organism *T. thermophilus*, TthPolX, contains a serine in the equivalent position of Asn^{513}. The lack of the asparagine in TthPolX restricts the error-prone insertion of 8-oxo-dGTP opposite dA by 10-fold (72). This is thought to be an adaptation to the higher levels of 8-oxo-dGTP in the dNTP pool expected at high temperatures. However, the absence of an asparagine residue at this position results in an imbalance in the efficiency of incorporation of purine and pyrimidine nucleotides (72), suggesting that acquiring an asparagine at this position is important for fidelity of incorporation when dealing with undamaged substrates. Ac-

cordingly, Asn^{513} appears to play a role in improving the purine/pyrimidine balance in Pol λ. Furthermore, our results demonstrate that Ala^{510} is also important for reducing the purine/pyrimindine bias. Owing to their larger surface area, purines have more stable base-stacking interactions than pyrimidines. Thus, direct interactions with the nucleobase appear to be relatively more important to stabilize the smaller pyrimidines. In that context, the energetics of the Ala^{510} interaction are likely to depend on the identity of the incoming nucleotide. At the same time, the hydrogen bond established by Asn^{513} appears to be critical to properly orient the incoming base. Thus, altering the Asn^{513} interaction in turn affects the Van der Waals contacts established by Ala^{510}. Accordingly, the effect of the double substitution on 8-oxo-dGMP/dTMP incorporation opposite dA is markedly different than the product of both individual single substitutions.

In all DNA polymerases, interactions with the incoming dNTP are essential for catalysis and selectivity. In the Pol λ active site, Ala^{510} and Asn^{513} cooperate to stabilize the incoming nucleotide. Our results highlight that dNTP binding involves multiple interactions and the relative importance of each interaction depends on the specific base being incorporated. Both Ala^{510} and Asn^{513} influence 8-oxo-dGMP incorporation as well as the balance between purine/pyrimidine incorporation. Thus, the increased catalytic efficiency of incorporation of undamaged nucleotides and purine/pyrimidine balance conferred by these residues comes thus at the price of an increased mutagenic risk in the presence of a significant pool of 8-oxo-dGTP. The described structures and kinetic results provide a framework for understanding 8-oxo-dGTP incorporation by DNA polymerases, and specifically in the context of the Pol λ active site. These new structural insights into the catalytic cycle for 8-oxo-dGTP incorporation by Pol λ will contribute to our understanding of the mutagenic potential of oxidized nucleotide pools, and the mechanisms by which DNA polymerases cope with and discriminate against these mutagenic events.

ACCESSION CODES

Atomic coordinates and structure factors for the pre-catalytic ternary complex and the post have been deposited in the Protein Data Bank with accession codes 4XA5, 4X5V and 4XUS.

SUPPLEMENTARY DATA

Supplementary Data are available at NAR Online.

ACKNOWLEDGEMENTS

The authors wish to thank all members of the Garcia-Diaz laboratory for insightful discussions and support, as well as Drs. Mark Lukin and Elena Yakubovskaya for oligonucleotide synthesis.

FUNDING

National Institutes of Health (NIH) [T32 GM092714 to M.J.B.]; NIH [ES022930 to K.E.G.]; NIH [GM100021 to M.G.D.]; Use of beamline X25 at the National Synchrotron Light Source; Brookhaven National Laboratory, was supported by the U.S. Department of Energy, Office of Science, Office of Basic Energy Sciences [DE-AC02-98CH10886]; Use of beamline 5.0.2 at the Advanced Light Source was supported by the Director, Office of Science, Office of Basic Energy Sciences, of the U.S. Department of Energy [DE-AC02–05CH11231]. Funding for open access charge: NIH [GM100021]; Use of the Stanford Synchrotron Radiation Lightsource, SLAC National Accelerator Laboratory, is supported by the U.S. Department of Energy, Office of Science, Office of Basic Energy Sciences under Contract No. DE-AC02-76SF00515. The SSRL Structural Molecular Biology Program is supported by the DOE Office of Biological and Environmental Research, and by the National Institutes of Health, National Institute of General Medical Sciences (including P41GM103393).

Conflict of interest statement. None declared.

REFERENCES

1. Neeley,W.L. and Essigmann,J.M. (2006) Mechanisms of formation, genotoxicity, and mutation of guanine oxidation products. *Chem. Res. Toxicol.*, **19**, 491–505.
2. Kamiya,H., Miura,K., Ishikawa,H., Inoue,H., Nishimura,S. and Ohtsuka,E. (1992) c-Ha-ras containing 8-hydroxyguanine at codon 12 induces point mutations at the modified and adjacent positions. *Cancer Res.*, **52**, 3483–3485.
3. Moriya,M. (1993) Single-stranded shuttle phagemid for mutagenesis studies in mammalian cells: 8-oxoguanine in DNA induces targeted G.C–>T.A transversions in simian kidney cells. *Proc. Natl. Acad. Sci. U.S.A.*, **90**, 1122–1126.
4. Kamiya,H., Murata-Kamiya,N., Koizume,S., Inoue,H., Nishimura,S. and Ohtsuka,E. (1995) 8-Hydroxyguanine (7,8-dihydro-8-oxoguanine) in hot spots of the c-Ha-ras gene: effects of sequence contexts on mutation spectra. *Carcinogenesis*, **16**, 883–889.
5. Le Page,F., Margot,A., Grollman,A.P., Sarasin,A. and Gentil,A. (1995) Mutagenicity of a unique 8-oxoguanine in a human Ha-ras sequence in mammalian cells. *Carcinogenesis*, **16**, 2779–2784.
6. Kamiya,H., Murata-Kamiya,N., Fujimuro,M., Kido,K., Inoue,H., Nishimura,S., Masutani,C., Hanaoka,F. and Ohtsuka,E. (1995) Comparison of incorporation and extension of nucleotides in vitro opposite 8-hydroxyguanine (7,8-dihydro-8-oxoguanine) in hot spots of the c-Ha-ras gene. *Jpn. J. Cancer Res.: Gann*, **86**, 270–276.
7. De Bont,R. and van Larebeke,N. (2004) Endogenous DNA damage in humans: a review of quantitative data. *Mutagenesis*, **19**, 169–185.
8. Pursell,Z.F., McDonald,J.T., Mathews,C.K. and Kunkel,T.A. (2008) Trace amounts of 8-oxo-dGTP in mitochondrial dNTP pools reduce DNA polymerase gamma replication fidelity. *Nucleic Acids Res.*, **36**, 2174–2181.
9. Maki,H. and Sekiguchi,M. (1992) MutT protein specifically hydrolyses a potent mutagenic substrate for DNA synthesis. *Nature*, **355**, 273–275.
10. Gad,H., Koolmeister,T., Jemth,A.S., Eshtad,S., Jacques,S.A., Strom,C.E., Svensson,L.M., Schultz,N., Lundback,T., Einarsdottir,B.O. *et al.* (2014) MTH1 inhibition eradicates cancer by preventing sanitation of the dNTP pool. *Nature*, **508**, 215–221.
11. Huber,K.V., Salah,E., Radic,B., Gridling,M., Elkins,J.M., Stukalov,A., Jemth,A.S., Gokturk,C., Sanjiv,K., Stromberg,K. *et al.* (2014) Stereospecific targeting of MTH1 by (S)-crizotinib as an anticancer strategy. *Nature*, **508**, 222–227.
12. Colussi,C., Parlanti,E., Degan,P., Aquilina,G., Barnes,D., Macpherson,P., Karran,P., Crescenzi,M., Dogliotti,E. and Bignami,M. (2002) The mammalian mismatch repair pathway removes DNA 8-oxodGMP incorporated from the oxidized dNTP pool. *Curr. Biol.: CB*, **12**, 912–918.
13. Satou,K., Kawai,K., Kasai,H., Harashima,H. and Kamiya,H. (2007) Mutagenic effects of 8-hydroxy-dGTP in live mammalian cells. *Free Radic. Biol. Med.*, **42**, 1552–1560.

14. Oda,Y., Uesugi,S., Ikehara,M., Nishimura,S., Kawase,Y., Ishikawa,H., Inoue,H. and Ohtsuka,E. (1991) Nmr-Studies of a DNA Containing 8-Hydroxydeoxyguanosine. *Nucleic Acids Res.*, **19**, 1407–1412.
15. Kouchakdjian,M., Bodepudi,V., Shibutani,S., Eisenberg,M., Johnson,F., Grollman,A.P. and Patel,D.J. (1991) NMR structural studies of the ionizing radiation adduct 7-hydro-8-oxodeoxyguanosine (8-oxo-7H-dG) opposite deoxyadenosine in a DNA duplex. 8-Oxo-7H-dG(syn).dA(anti) alignment at lesion site. *Biochemistry*, **30**, 1403–1412.
16. McAuley-Hecht,K.E., Leonard,G.A., Gibson,N.J., Thomson,J.B., Watson,W.P., Hunter,W.N. and Brown,T. (1994) Crystal structure of a DNA duplex containing 8-hydroxydeoxyguanine-adenine base pairs. *Biochemistry*, **33**, 10266–10270.
17. Lipscomb,L.A., Peek,M.E., Morningstar,M.L., Verghis,S.M., Miller,E.M., Rich,A., Essigmann,J.M. and Williams,L.D. (1995) X-ray structure of a DNA decamer containing 7,8-dihydro-8-oxoguanine. *Proc. Natl. Acad. Sci. U.S.A.*, **92**, 719–723.
18. Einolf,H.J., Schnetz-Boutaud,N. and Guengerich,F.P. (1998) Steady-state and pre-steady-state kinetic analysis of 8-oxo-7,8-dihydroguanosine triphosphate incorporation and extension by replicative and repair DNA polymerases. *Biochemistry*, **37**, 13300–13312.
19. Miller,H., Prasad,R., Wilson,S.H., Johnson,F. and Grollman,A.P. (2000) 8-oxodGTP incorporation by DNA polymerase beta is modified by active-site residue Asn279. *Biochemistry*, **39**, 1029–1033.
20. Shimizu,M., Gruz,P., Kamiya,H., Kim,S.R., Pisani,F.M., Masutani,C., Kanke,Y., Harashima,H., Hanaoka,F. and Nohmi,T. (2003) Erroneous incorporation of oxidized DNA precursors by Y-family DNA polymerases. *EMBO Rep.*, **4**, 269–273.
21. Hanes,J.W., Thal,D.M. and Johnson,K.A. (2006) Incorporation and replication of 8-oxo-deoxyguanosine by the human mitochondrial DNA polymerase. *J. Biol. Chem.*, **281**, 36241–36248.
22. Yamada,M., Nunoshiba,T., Shimizu,M., Gruz,P., Kamiya,H., Harashima,H. and Nohmi,T. (2006) Involvement of Y-family DNA polymerases in mutagenesis caused by oxidized nucleotides in Escherichia coli. *J. Bacteriol.*, **188**, 4992–4995.
23. Brown,J.A., Duym,W.W., Fowler,J.D. and Suo,Z. (2007) Single-turnover kinetic analysis of the mutagenic potential of 8-oxo-7,8-dihydro-2′-deoxyguanosine during gap-filling synthesis catalyzed by human DNA polymerases lambda and beta. *J. Mol. Biol.*, **367**, 1258–1269.
24. Shimizu,M., Gruz,P., Kamiya,H., Masutani,C., Xu,Y., Usui,Y., Sugiyama,H., Harashima,H., Hanaoka,F. and Nohmi,T. (2007) Efficient and erroneous incorporation of oxidized DNA precursors by human DNA polymerase eta. *Biochemistry*, **46**, 5515–5522.
25. Katafuchi,A., Sassa,A., Niimi,N., Gruz,P., Fujimoto,H., Masutani,C., Hanaoka,F., Ohta,T. and Nohmi,T. (2010) Critical amino acids in human DNA polymerases eta and kappa involved in erroneous incorporation of oxidized nucleotides. *Nucleic Acids Res.*, **38**, 859–867.
26. Zaccolo,M., Williams,D.M., Brown,D.M. and Gherardi,E. (1996) An approach to random mutagenesis of DNA using mixtures of triphosphate derivatives of nucleoside analogues. *J. Mol. Biol.*, **255**, 589–603.
27. Svilar,D., Goellner,E.M., Almeida,K.H. and Sobol,R.W. (2011) Base excision repair and lesion-dependent subpathways for repair of oxidative DNA damage. *Antioxid. Redox Signal.*, **14**, 2491–2507.
28. Aburatani,H., Hippo,Y., Ishida,T., Takashima,R., Matsuba,C., Kodama,T., Takao,M., Yasui,A., Yamamoto,K. and Asano,M. (1997) Cloning and characterization of mammalian 8-hydroxyguanine-specific DNA glycosylase/apurinic, apyrimidinic lyase, a functional mutM homologue. *Cancer Res.*, **57**, 2151–2156.
29. Williams,S.D. and David,S.S. (1998) Evidence that MutY is a monofunctional glycosylase capable of forming a covalent Schiff base intermediate with substrate DNA. *Nucleic Acids Res.*, **26**, 5123–5133.
30. Zharkov,D.O. and Grollman,A.P. (1998) MutY DNA glycosylase: base release and intermediate complex formation. *Biochemistry*, **37**, 12384–12394.
31. Williams,S.D. and David,S.S. (1999) Formation of a Schiff base intermediate is not required for the adenine glycosylase activity of Escherichia coli MutY. *Biochemistry*, **38**, 15417–15424.
32. Batra,V.K., Beard,W.A., Hou,E.W., Pedersen,L.C., Prasad,R. and Wilson,S.H. (2010) Mutagenic conformation of 8-oxo-7,8-dihydro-2′-dGTP in the confines of a DNA polymerase active site. *Nat. Struct. Mol. Biol.*, **17**, 889–890.
33. Freudenthal,B.D., Beard,W.A., Perera,L., Shock,D.D., Kim,T., Schlick,T. and Wilson,S.H. (2014) Uncovering the polymerase-induced cytotoxicity of an oxidized nucleotide. *Nature*, **517**, 635–639.
34. Maga,G., Villani,G., Crespan,E., Wimmer,U., Ferrari,E., Bertocci,B. and Hubscher,U. (2007) 8-oxo-guanine bypass by human DNA polymerases in the presence of auxiliary proteins. *Nature*, **447**, 606–608.
35. Markkanen,E., Castrec,B., Villani,G. and Hubscher,U. (2012) A switch between DNA polymerases delta and lambda promotes error-free bypass of 8-oxo-G lesions. *Proc. Natl. Acad. Sci. U.S.A.*, **109**, 20401–20406.
36. Markkanen,E., Dorn,J. and Hubscher,U. (2013) MUTYH DNA glycosylase: the rationale for removing undamaged bases from the DNA. *Front. Genet.*, **4**, 18.
37. Fan,W. and Wu,X. (2004) DNA polymerase lambda can elongate on DNA substrates mimicking non-homologous end joining and interact with XRCC4-ligase IV complex. *Biochem. Biophys. Res. Commun.*, **323**, 1328–1333.
38. Lee,J.W., Blanco,L., Zhou,T., Garcia-Diaz,M., Bebenek,K., Kunkel,T.A., Wang,Z. and Povirk,L.F. (2004) Implication of DNA polymerase lambda in alignment-based gap filling for nonhomologous DNA end joining in human nuclear extracts. *J. Biol. Chem.*, **279**, 805–811.
39. Nick McElhinny,S.A., Havener,J.M., Garcia-Diaz,M., Juarez,R., Bebenek,K., Kee,B.L., Blanco,L., Kunkel,T.A. and Ramsden,D.A. (2005) A gradient of template dependence defines distinct biological roles for family X polymerases in nonhomologous end joining. *Mol. Cell*, **19**, 357–366.
40. Capp,J.P., Boudsocq,F., Bertrand,P., Laroche-Clary,A., Pourquier,P., Lopez,B.S., Cazaux,C., Hoffmann,J.S. and Canitrot,Y. (2006) The DNA polymerase lambda is required for the repair of non-compatible DNA double strand breaks by NHEJ in mammalian cells. *Nucleic Acids Res.*, **34**, 2998–3007.
41. Akopiants,K., Zhou,R.Z., Mohapatra,S., Valerie,K., Lees-Miller,S.P., Lee,K.J., Chen,D.J., Revy,P., de Villartay,J.P. and Povirk,L.F. (2009) Requirement for XLF/Cernunnos in alignment-based gap filling by DNA polymerases lambda and mu for nonhomologous end joining in human whole-cell extracts. *Nucleic Acids Res.*, **37**, 4055–4062.
42. Garcia-Diaz,M., Bebenek,K., Krahn,J.M., Blanco,L., Kunkel,T.A. and Pedersen,L.C. (2004) A structural solution for the DNA polymerase lambda-dependent repair of DNA gaps with minimal homology. *Mol. Cell*, **13**, 561–572.
43. Kabsch,W. (2010) Xds. *Acta Crystallogr. Sect. D, Biol. Crystallogr.*, **66**, 125–132.
44. Evans,P.R. and Murshudov,G.N. (2013) How good are my data and what is the resolution? *Acta Crystallogr. Sect. D, Biol. Crystallogr.*, **69**, 1204–1214.
45. Vonrhein,C., Flensburg,C., Keller,P., Sharff,A., Smart,O., Paciorek,W., Womack,T. and Bricogne,G. (2011) Data processing and analysis with the autoPROC toolbox. *Acta Crystallogr. Sect. D, Biol. Crystallogr.*, **67**, 293–302.
46. McCoy,A.J., Grosse-Kunstleve,R.W., Adams,P.D., Winn,M.D., Storoni,L.C. and Read,R.J. (2007) Phaser crystallographic software. *J. Appl. Crystallogr.*, **40**, 658–674.
47. Garcia-Diaz,M., Bebenek,K., Krahn,J.M., Kunkel,T.A. and Pedersen,L.C. (2005) A closed conformation for the Pol lambda catalytic cycle. *Nat. Structu. Mol. Biol.*, **12**, 97–98.
48. Emsley,P., Lohkamp,B., Scott,W.G. and Cowtan,K. (2010) Features and development of Coot. *Acta Crystallogr. Sect. D, Biol. Crystallogr.*, **66**, 486–501.
49. Zwart,P.H., Afonine,P.V., Grosse-Kunstleve,R.W., Hung,L.W., Ioerger,T.R., McCoy,A.J., McKee,E., Moriarty,N.W., Read,R.J., Sacchettini,J.C. *et al.* (2008) Automated structure solution with the PHENIX suite. *Methods Mol. Biol.*, **426**, 419–435.
50. Murshudov,G.N., Skubak,P., Lebedev,A.A., Pannu,N.S., Steiner,R.A., Nicholls,R.A., Winn,M.D., Long,F. and Vagin,A.A. (2011) REFMAC5 for the refinement of macromolecular crystal structures. *Acta Crystallogr. Sect. D, Biol. Crystallogr.*, **67**, 355–367.
51. Smart,O.S., Womack,T.O., Flensburg,C., Keller,P., Paciorek,W., Sharff,A., Vonrhein,C. and Bricogne,G. (2012) Exploiting structure

similarity in refinement: automated NCS and target-structure restraints in BUSTER. *Acta Crystallogr. Sect. D, Biol. Crystallogra.*, **68**, 368–380.
52. Karplus,P.A. and Diederichs,K. (2012) Linking crystallographic model and data quality. *Science*, **336**, 1030–1033.
53. Sawaya,M.R. (2014) Methods to refine macromolecular structures in cases of severe diffraction anisotropy. *Methods Mol. Biolo.*, **1091**, 205–214.
54. Chen,V.B., Arendall,W.B. 3rd, Headd,J.J., Keedy,D.A., Immormino,R.M., Kapral,G.J., Murray,L.W., Richardson,J.S. and Richardson,D.C. (2010) MolProbity: all-atom structure validation for macromolecular crystallography. *Acta Crystallogr. Sect. D, Biol. Crystallogr.*, **66**, 12–21.
55. Vaguine,A.A., Richelle,J. and Wodak,S.J. (1999) SFCHECK: a unified set of procedures for evaluating the quality of macromolecular structure-factor data and their agreement with the atomic model. *Acta Crystallogra. Sect. D, Biol. Crystallogr.*, **55**, 191–205.
56. Cruickshank,D. (1949) The accuracy of electron-density maps in X-ray analysis with special reference to dibenzyl. *Acta Crystallogr.*, **2**, 65–82.
57. Agarwal,R. (1978) A new least-squares refinement technique based on the fast Fourier transform algorithm. *Acta Crystallogr. Sect. A*, **34**, 791–809.
58. Murshudov,G.N., Vagin,A.A. and Dodson,E.J. (1997) Refinement of Macromolecular Structures by the Maximum-Likelihood Method. *Acta Crystallogr. Sect. D*, **53**, 240–255.
59. Bebenek,K., Pedersen,L.C. and Kunkel,T.A. (2011) Replication infidelity via a mismatch with Watson-Crick geometry. *Proc. Natl. Acad. Sci. U.S.A.*, **108**, 1862–1867.
60. Garcia-Diaz,M., Bebenek,K., Sabariegos,R., Dominguez,O., Rodriguez,J., Kirchhoff,T., Garcia-Palomero,E., Picher,A.J., Juarez,R., Ruiz,J.F. *et al.* (2002) DNA polymerase lambda, a novel DNA repair enzyme in human cells. *J. Biol. Chem.*, **277**, 13184–13191.
61. Brown,J.A., Pack,L.R., Sherrer,S.M., Kshetry,A.K., Newmister,S.A., Fowler,J.D., Taylor,J.S. and Suo,Z. (2010) Identification of critical residues for the tight binding of both correct and incorrect nucleotides to human DNA polymerase lambda. *J. Mol. Biol.*, **403**, 505–515.
62. Eom,S.H., Wang,J. and Steitz,T.A. (1996) Structure of Taq polymerase with DNA at the polymerase active site. *Nature*, **382**, 278–281.
63. Kiefer,J.R., Mao,C., Braman,J.C. and Beese,L.S. (1998) Visualizing DNA replication in a catalytically active Bacillus DNA polymerase crystal. *Nature*, **391**, 304–307.
64. Krahn,J.M., Beard,W.A., Miller,H., Grollman,A.P. and Wilson,S.H. (2003) Structure of DNA polymerase beta with the mutagenic DNA lesion 8-oxodeoxyguanine reveals structural insights into its coding potential. *Structure*, **11**, 121–127.
65. Hsu,G.W., Ober,M., Carell,T. and Beese,L.S. (2004) Error-prone replication of oxidatively damaged DNA by a high-fidelity DNA polymerase. *Nature*, **431**, 217–221.
66. Brieba,L.G., Eichman,B.F., Kokoska,R.J., Doublie,S., Kunkel,T.A. and Ellenberger,T. (2004) Structural basis for the dual coding potential of 8-oxoguanosine by a high-fidelity DNA polymerase. *EMBO J.*, **23**, 3452–3461.
67. Vasquez-Del Carpio,R., Silverstein,T.D., Lone,S., Swan,M.K., Choudhury,J.R., Johnson,R.E., Prakash,S., Prakash,L. and Aggarwal,A.K. (2009) Structure of human DNA polymerase kappa inserting dATP opposite an 8-OxoG DNA lesion. *PLoS One*, **4**, e5766.
68. Beard,W.A. and Wilson,S.H. (2000) Structural design of a eukaryotic DNA repair polymerase: DNA polymerase beta. *Mutat. Res.*, **460**, 231–244.
69. Vande Berg,B.J., Beard,W.A. and Wilson,S.H. (2001) DNA structure and aspartate 276 influence nucleotide binding to human DNA polymerase beta. Implication for the identity of the rate-limiting conformational change. *J. Biol. Chem.*, **276**, 3408–3416.
70. Garcia-Diaz,M., Bebenek,K., Krahn,J.M., Pedersen,L.C. and Kunkel,T.A. (2007) Role of the catalytic metal during polymerization by DNA polymerase lambda. *DNA Repair*, **6**, 1333–1340.
71. Werneburg,B.G., Ahn,J., Zhong,X., Hondal,R.J., Kraynov,V.S. and Tsai,M.D. (1996) DNA polymerase beta: pre-steady-state kinetic analysis and roles of arginine-283 in catalysis and fidelity. *Biochemistry*, **35**, 7041–7050.
72. Garrido,P., Mejia,E., Garcia-Diaz,M., Blanco,L. and Picher,A.J. (2014) The active site of TthPolX is adapted to prevent 8-oxo-dGTP misincorporation. *Nucleic Acids Res.*, **42**, 534–543.
73. Fraga,C.G., Shigenaga,M.K., Park,J.W., Degan,P. and Ames,B.N. (1990) Oxidative damage to DNA during aging: 8-hydroxy-2′-deoxyguanosine in rat organ DNA and urine. *Proc. Natl. Acad. Sci. U.S.A.*, **87**, 4533–4537.